

## Predictability Characteristics of Landfalling Cyclones along the North American West Coast

LYNN A. MCMURDIE

*Department of Atmospheric Sciences, University of Washington, Seattle, Washington*

BRIAN ANCELL

*Department of Geosciences, Texas Tech University, Lubbock, Texas*

(Manuscript received 24 April 2013, in final form 29 August 2013)

### ABSTRACT

The predictability of North Pacific cyclones can vary widely, from highly accurate prediction of storm intensity and location to forecast position errors of hundreds of kilometers and central pressure errors of tens of hectopascals. In this study, a Weather Research and Forecasting Model (WRF) ensemble Kalman filter is used to investigate predictability of landfalling cyclones on the west coast of North America over two winter seasons (2008/09 and 2009/10). Predictability is defined as the ensemble spread of cyclone central pressure at the final forecast time (24 h) where large spread means low predictability. Both ensemble spread and ensemble initial-condition sensitivity are examined for a wide variety of cyclones that occurred during the two seasons. Storms that are deepening and track from the southwest exhibit the largest ensemble initial-condition sensitivity and highest ensemble spread compared to decaying storms and storms that track from other directions. Storms that end south of 40°N, typically slow moving storms from the northwest, exhibit higher predictability regardless of whether or not they are deepening or decaying. Cyclones with large ensemble spread and low sensitivity are mature cyclones whose low predictability likely results from large initial-condition spread instead of large perturbation growth. These results highlight particular synoptic situations and cyclone characteristics that are associated with low predictability and can potentially be used to improve forecasts through improved observational coverage.

### 1. Introduction

North Pacific storms impact the west coast of North America, from California to southeast Alaska, and bring strong winds, precipitation, and large mountain snowfall that result in significant societal and economic impacts. The success of numerical forecasts of these storms can vary widely, from highly accurate prediction of storm location and intensity to storm position errors on the order of hundreds of kilometers and intensity errors of tens of hectopascals (McMurdie and Mass 2004). Recent studies have shown that this region typically experiences larger short-term (<72 h) forecast errors of sea level pressure and cyclone position compared to other regions such as continental United States and the east coast of

North America (Wedam et al. 2009; Charles and Colle 2009). Although possible causes for these forecast errors were not addressed in those studies, McMurdie and Mass (2004) showed that initial-condition error played a significant role in the forecast errors for a particular deepening landfalling cyclone.

McMurdie and Casola (2009) related forecast errors of pressure and temperature in the National Centers for Environmental Prediction (NCEP) Global Forecast System (GFS) and North American Mesoscale Model (NAM) along the west coast of North America to large-scale flow patterns. They found that the Rockies Ridge regime, which is characterized by a ridge near the axis of the Rocky Mountains and nearly zonal flow across the Pacific, experiences the highest magnitude and frequency of large sea level pressure errors. The Coastal Ridge regime, which exhibits a ridge aligned with the North American west coast, experiences the highest magnitude and frequency of large 2-m minimum temperature errors. They also found that days with strong

---

*Corresponding author address:* Lynn McMurdie, Department of Atmospheric Sciences, University of Washington, Box 351640, Seattle, WA 98195.  
E-mail: mcmurdie@atmos.washington.edu

upper-level jet strength were more likely to experience large forecast errors of sea level pressure along the west coast than days with weaker upper-level winds. Colle and Charles (2011) examined the spatial distribution and evolution of sea level pressure forecast errors across North America and adjacent oceans in the NCEP GFS model. Among their findings for the North and eastern Pacific regions, they found that cyclones forecasted to be weaker than observed were more likely to occur in the 35°–45°N latitude belt and cyclones that were forecasted to be stronger than observed were found north of 45°N. Both Colle and Charles (2011) and McMurdie and Casola (2009) used similar time periods for their study, roughly 2002–08.

Ensemble forecasting techniques are currently gaining popularity both operationally and for research applications. Some benefits of ensembles are that the ensemble mean can improve upon the skill of deterministic forecasts (Kalnay 2002), and that they provide straightforward and flow dependent estimates of analysis and forecast uncertainty. An ensemble system has an appropriate amount of spread if the ratio of the square forecast errors to the forecast and observation variance is 1 (Murphy 1988; Houtekamer et al. 2005), suggesting the spread of a calibrated ensemble can serve as a proxy for predictability. Here a primary goal is to understand how the spread (and subsequent predictability) of North American landfalling midlatitude cyclones varies for different flow patterns (as in McMurdie and Casola 2009, but at smaller scales) and cyclone characteristics (e.g., deepening versus decaying) within a well-calibrated ensemble system.

Several studies have investigated predictability from a purely dynamical growth perspective. Klinker et al. (1998) introduced “key analysis errors,” which identified areas based on adjoint sensitivity where perturbation growth would be largest. Reynolds and Gelaro (2001) showed preferential regions of the largest sensitivity of 48-h forecast error over a 4-yr period, and even showed interannual variability of forecast error sensitivity that was linked to the ENSO cycle. Shapiro et al. (2001) also demonstrated larger forecast errors (defined as errors in the total energy norm) for the La Niña year of 1998/99 compared to the El Niño year of 1997/98.

A major advantage of examining predictability within an ensemble framework is that both ensemble sensitivity (Ansell and Hakim 2007; Hakim and Torn 2008; Torn and Hakim 2008b) and analysis/forecast spread can be calculated. Since ensemble sensitivity can provide a measure of the dynamical error growth of initial-time perturbations (Ansell and Hakim 2007), and the likely initial-time perturbations (which can be interpreted as the likely errors in a calibrated ensemble system) can be

described by ensemble analysis covariances, the contributions from these two factors to predictability can be explored. For example, large forecast spread could be a result of small initial spread and large dynamical growth, or large initial spread and small dynamical growth. By appropriately characterizing these quantities with an ensemble, we seek to relate not only predictability to different atmospheric flows, but also explore some of the possible causes. In turn, since initial-time spread (which is defined as the variance in the analysis contained within the ensemble) can be reduced through data assimilation, this study might reveal the types of flows for which enhanced observations could be most beneficial. Such locations were investigated by Ansell and McMurdie (2013), who found preferential locations relative to forecast oceanic cyclones where targeted observations would reduce forecast variance the most for certain types of storms. Results here might help explain the persistent targeting locations found in Ansell and McMurdie (2013) from a flow regime perspective.

We use an ensemble Kalman filter (EnKF; Evensen 1994) to investigate the predictability, ensemble sensitivity, and spread characteristics of landfalling cyclones on the west coast of North America over two winter seasons. In this study, we define predictability to be the ensemble spread at the final forecast time (24 h), where low predictability exhibits large ensemble spread and high predictability exhibits small ensemble spread. We assume that the initial-time spread in the calibrated ensemble is able to characterize analysis error, such that large (small) analysis spread exhibits a larger (smaller) likelihood of initial-condition error. Specifically, we are addressing the following two questions: Are there common characteristics among storms with similar predictability (i.e., spread)? What is the role of dynamical perturbation growth versus initial-time spread for the least (and most) predictable cyclones? The organization of this paper is as follows: section 2 provides a background on ensemble sensitivity and its role in this study, section 3 provides the methodology used in our experiments, section 4 give results and discussion, and section 5 provides a summary and conclusions.

## 2. Background

Ensemble sensitivity reveals weather features at the initial time to which a chosen forecast response function is sensitive. As described in Ansell and Hakim (2007), it differs from adjoint sensitivity in that it reveals features of the flow, such as upper-level geopotential height troughs or baroclinic zones, which are important to the forecast response function. Adjoint sensitivity analysis, alternatively, reveals the fastest-growing perturbations,

and in cases of cyclogenesis, generally highlights lower-tropospheric, upshear-tilted regions (Langland et al. 1995; Gelaro et al. 1998; Hoskins et al. 2000; Badger and Hoskins 2001) that are separated from coherent features such as the driving upper-level trough. The work of Piccolo (2011) elaborates on this difference through the examination of errors modeled by ensemble covariances that grew rapidly since they were able to project onto rapidly growing modes. In fact, Ancell and Hakim (2007) describe that the key relationship between the two types of sensitivity is that ensemble-sensitive regions are coherent flow structures that are collectively related to adjoint-sensitive regions through ensemble covariances. Thus, within an ensemble framework, ensemble sensitivity still reveals the flow features that if perturbed would most alter the response function, and can appropriately be referred to as “intrinsic predictability.”

Ensemble sensitivity has been applied successfully in previous studies involving cyclones to investigate the sensitivity of African easterly waves to analysis errors (Torn 2010), to understand the important features of the flow relative to the predictability of North American landfalling midlatitude cyclones (Ancell and Hakim 2007), to diagnose the important features relevant to both cyclone track and intensity forecasts (Zheng et al. 2013), and to explore whether an ensemble sensitivity approach is useful for medium-range (~1 week) forecasts (Chang et al. 2013). In addition, Matsueda et al. (2011) examined the predictability of an atmospheric blocking event, and found sensitivity to a cutoff cyclone in the North Pacific through the inspection of a multi-model ensemble.

The ensemble sensitivity of a scalar response function  $R$  with respect to a single initial-time atmospheric variable (e.g., surface temperature  $T_i$  at a single model grid point) is calculated using the following equation:

$$\partial R/\partial T_i = CV_{R,T_i}/V_{T_i}, \quad (1)$$

where  $\partial R/\partial T_i$  is the ensemble sensitivity of  $R$  to  $T_i$ ,  $CV_{R,T_i}$  represents the covariance between  $R$  and  $T_i$ , and  $V_{T_i}$  represents the variance of  $T_i$ . By performing this calculation with respect to the entire initial-time atmospheric state, the entire ensemble sensitivity field can be obtained. The value of the ensemble sensitivity is equivalent to the slope of a linear regression of  $R$  onto each initial-time model variable. Since this linear relationship is used, strong nonlinear perturbation evolution reduces the accuracy and usefulness of ensemble sensitivity (Ancell and Hakim 2007). On synoptic scales, nonlinearity has been shown to become significant after

1–2 days (Gilmour et al. 2001; Ancell and Mass 2006; Ancell 2013), a timeframe within which our study is performed.

In this study, we aim to relate not only large and small forecast spread (and predictability) associated with landfalling midlatitude cyclones to atmospheric flow characteristics, but also the contributing factors to the forecast spread. These contributing factors were presented in section 1 as 1) the potential for dynamical growth of perturbations (referred to hereafter as the intrinsic predictability), and 2) the initial-time ensemble spread that characterizes the perturbations. This viewpoint is justified by Errico (1997), who showed forecast perturbations (scalar  $\Delta R$ ) can be estimated through the projection of initial-time atmospheric perturbations (column vector  $\Delta \mathbf{x}$ ) onto the adjoint sensitivity with respect to initial time (column vector  $\partial R/\partial \mathbf{x}$ ):

$$\Delta R = \partial R/\partial \mathbf{x}^T \times \Delta \mathbf{x}. \quad (2)$$

We extend this idea to an ensemble system, using ensemble sensitivity instead of adjoint sensitivity to represent the intrinsic predictability, and allowing the initial-time ensemble spread to characterize the analysis perturbations. Through this interpretation, we aim to thus understand the contributions that both the intrinsic predictability and the initial-time spread have on the least (and most) predictable flow patterns.

### 3. Methodology

A 36-km, 38-vertical level Weather Research and Forecasting Model (WRF; Skamarock et al. 2008) EnKF configuration (domain shown in Fig. 1) is used in this study. This EnKF is an ensemble square root filter (Whitaker and Hamill 2002) that assimilates observations serially and comprises 80 members. Observations are assimilated on a 6-h cycle and include the following: satellite cloud-track winds (~4000 cycle<sup>-1</sup>); Aircraft Communication, Addressing, and Reporting System (ACARS) aircraft temperature and wind observations (~4000 cycle<sup>-1</sup>); rawinsonde temperature, wind, and moisture observations (~1500 cycle<sup>-1</sup>); and surface wind, temperature, and altimeter observations (~6000 cycle<sup>-1</sup>). No radiance observations are assimilated. The EnKF data assimilation parameters used here are the same as those calibrated on a similar grid in Torn and Hakim (2008a), and are thus considered appropriate for this study. These parameters include an inflation factor to prevent ensemble underdispersiveness and filter divergence (Anderson and Anderson 1999), as well as a horizontal localization radius to reduce the influence of spurious long-range correlations (Gaspari and Cohn

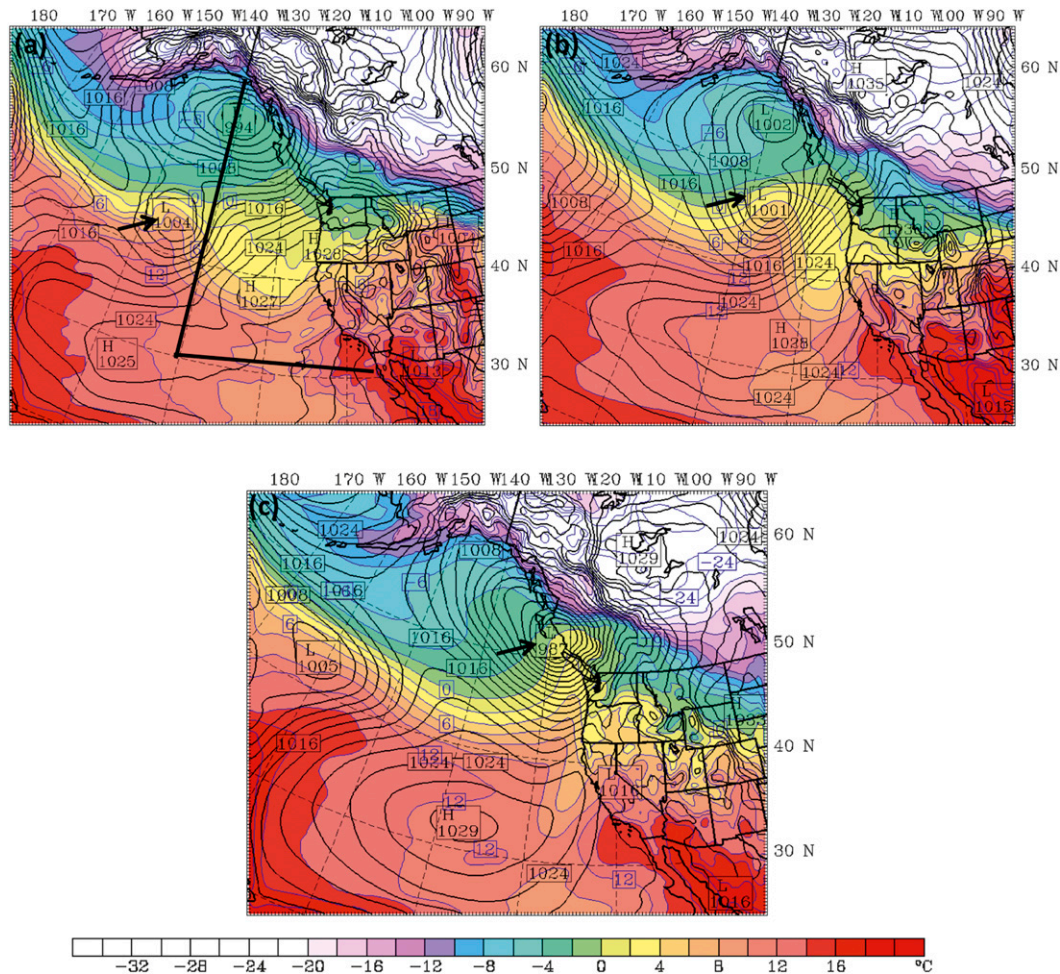


FIG. 1. Sea level pressure (black contours, every 2 hPa) and 925-hPa temperature (shaded) from the EnKF model run initialized on 0600 UTC 30 Dec 2008 valid at forecast hour (a) 0, (b) 12, and (c) 24. The heavy black arrow indicates the position of the deepening cyclone. The “offshore zone” is indicated by heavy black lines in (a).

1999). The 36-km EnKF obtains its boundary conditions through the fixed covariance method of Torn et al. (2006).

Forecasts are produced from each analysis to provide both the background (6-h forecast) for the next assimilation cycle, as well as the extended forecasts (out to 48 h) used to examine predictability of landfalling cyclones. Version 3.0.1.1 of WRF is used with the following model physics: the Mellor–Yamada–Janjic (MYJ) planetary boundary layer scheme (Janjic 1990, 1996, 2002), the Kain–Fritsch cumulus parameterization (Kain and Fritsch 1990, 1993), the Noah land surface model (Chen and Dudhia 2001), WRF single-moment 3-class microphysics scheme (Hong et al. 2004), the Rapid Radiative Transfer Model (RRTM) longwave radiation scheme (Mlawer et al. 1997), and the Dudhia shortwave radiation scheme (Dudhia 1989). The EnKF is cycled, and extended forecasts produced, for two winter seasons:

October–March 2008/09 and 2009/10. For each season, a 1-week spinup period involving the full suite of observations is run during the last week in September to allow the EnKF to acquire flow dependence prior to the start of each winter. The EnKF is initialized at the beginning of the spinup periods using a random draw from the climatological covariances within the WRF three-dimensional variational data assimilation system (WRFVAR; Barker et al. 2012).

Cyclones are identified within all 12–48-h forecasts through an algorithm that locates the minima in the sea level pressure field. This scheme searches for grid points at which the value of sea level pressure is less than that at each adjacent point. Each identified minima are verified by visual inspection to insure that the algorithm picked out minima that were truly cyclones (i.e., a closed circulation with minima with at least one or two contours of sea level pressure around it) and not a relative minimum

of sea level pressure between two surface high pressure centers.

For this study, a landfalling west coast North American cyclone is defined as a cyclone found within the “off-shore zone,” east of 140°W to the coast and between 30° and 60°N (see Fig. 1), at the 24-h forecast time in the ensemble mean sea level pressure field. The response function used to diagnose the cyclones for the sensitivity and spread calculations is defined as the average sea level pressure in a  $7 \times 7$  (216 km  $\times$  216 km) model grid box centered on the cyclone at the minimum in sea level pressure. So, unlike some other studies, the response function is not defined in terms of a specific geographical location, such as the west coast of Oregon, but is defined in terms of the 24-h forecast of the ensemble mean position of the cyclone itself. The total number of forecasts of cyclones included in the study for the 2008/09 and 2009/10 winter seasons is 331. An individual cyclone can be sampled several times, since a typical cyclone would be within the “coastal zone” for 1–2 days. Therefore the 331 forecasts represent approximately 60–80 individual storms.

For each cyclone, the 24-h deepening rate, storm speed, and storm track is calculated from the ensemble mean sea level pressure fields for the particular forecast run, and not from observations. So, the actual deepening rate and storm track may differ slightly from the forecast runs in this study. Only cyclones that could be tracked over the full 24 h by the automated tracking algorithm were included in the study. The 24-h deepening rate, speed, and track were calculated using the position and central pressure of the ensemble mean cyclone at 0 and 24 h.

The ensemble sensitivity of the 24-h response function for each cyclone is calculated with respect to initial geopotential height at all model levels, and with respect to initial sea level pressure. Once the full sensitivity field associated with each cyclone is calculated, the maximum absolute value of the sensitivity for each variable is used to represent the largest potential for perturbation growth (intrinsic predictability). The spread of the response function is simply the standard deviation calculated from the 24-h ensemble forecasts of the response function. Since it is found for many cyclones that the relative maximum sensitivity values are independent of level (the same cyclones show relative minima in the sensitivity fields for all levels, not shown), the maximum values of sensitivity with respect to SLP are used in this study as a proxy for intrinsic predictability. It should be noted that other variables, such as winds or temperature, could be used in both the response function and the initial state variables to which sensitivity is calculated. Here, however, we limit our experiments to that of SLP

for both the response function and sensitivity, allowing the results to motivate future examination of other variables, and keeping this study to a reasonable length. For different groups of cyclones (e.g., all deepening cyclones), the maximum absolute value of sensitivity for each cyclone were averaged together and compared to other groups of cyclones. The same process was used for maximum ensemble spread.

Confidence intervals, or error bars, are displayed in many of the results. Two sets of error bars are used. The first set represents 95% confidence interval for the entire dataset (not segregated by category) and the second set represents the 95% confidence interval for a particular group or category (i.e., decaying cyclones tracking from the southwest). For the mean ensemble sensitivity or mean ensemble spread calculations, the error bars are given by

$$CI = t_{\text{crit}} \sigma / \sqrt{N - 1}, \quad (3)$$

where CI refers to the confidence interval, and  $\sigma$  and  $N$  are the standard deviation and the total number of cases, respectively, for the entire dataset (first group of error bars) or the standard deviation and number of days of the category (second group of error bars). The critical  $t$  value ( $t_{\text{crit}}$ ) is computed from a  $t$  distribution for a confidence interval of 0.975 and the degrees of freedom equal to the number of cases divided by 2, as in McMurdie and Casola (2009). Following that study, we focus the discussion of the results where the mean estimate associated with a category is not included in the confidence interval of the mean estimated associated with the entire dataset, and vice versa, and cases where two sets of confidence intervals do not overlap. These two cases indicate that the error statistics associated with a particular category are meaningful and are highly unlikely to be replicated from random sampling of the dataset.

## 4. Results and discussion

### a. Cyclone of 30 December 2008

An example of a deepening landfalling cyclone is shown in Figs. 1 and 2. In Fig. 1, the ensemble mean sea level pressure field at forecast hours 0, 12, and 24 for the EnKF model run initialized at 0600 UTC 30 December 2008 is shown. The cyclone deepens over the 24-h forecast from 1004 to 987 hPa. The cyclone travels from the southwest to the northeast and at the 24-h forecast time, it is positioned just off the northern tip of Vancouver Island. This type of cyclone would typically bring significant precipitation and wind to the Pacific Northwest and southern British Columbia. The exact track of

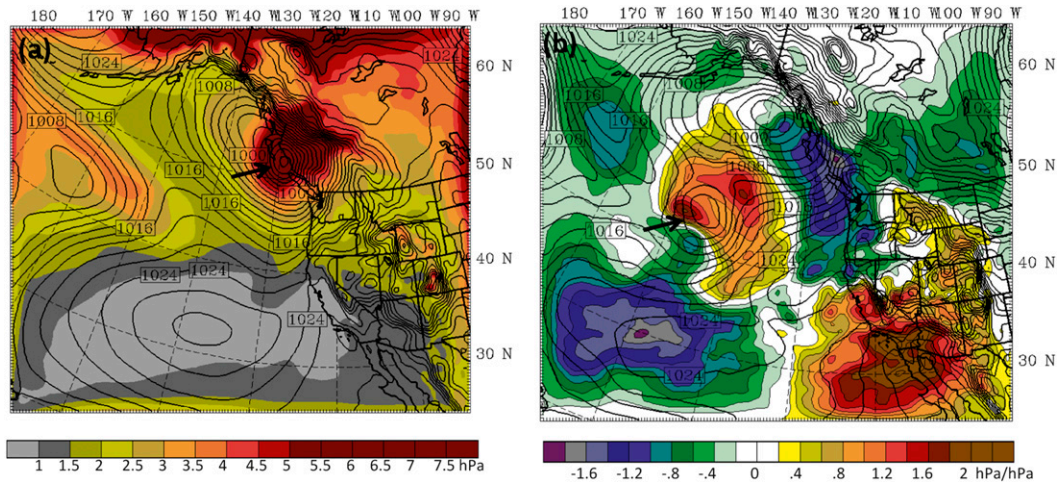


FIG. 2. (a) Ensemble spread of sea level pressure at 24 h forecast (shaded) and the ensemble mean sea level pressure (contours, every 2 hPa) initialized 0600 UTC 30 Dec 2008. The maximum ensemble spread in the vicinity of the deepening cyclone is greater than 6 hPa and is indicated with the bold black arrow. (b) Ensemble sensitivity of the cyclone central pressure at the final forecast time (24 h) to the initial-time sea level pressure field (shaded in  $\text{hPa hPa}^{-1}$ ) and initial sea level pressure field (black contours, every 2 hPa). A region of high sensitivity (greater than  $1 \text{ hPa hPa}^{-1}$ ) and a maximum of  $1.7 \text{ hPa hPa}^{-1}$  is found near the initial position of the incipient cyclone as indicated with the bold black arrow.

a cyclone of this nature is important to be able to forecast accurately since strong winds in highly populated areas of the Puget Sound Lowlands and Vancouver, British Columbia, are sensitive to the location and track of cyclones. If the cyclone were to track farther south by about 100 km or so, the potential for strong winds in the Puget Sound region would be high (Mass and Dotson 2010).

In Fig. 2, the ensemble spread at 24 h and the ensemble sensitivity of the forecast of cyclone central pressure to the initial sea level pressure field are shown. The ensemble spread is large in the vicinity of the forecast low with values well over 6 hPa indicating that the various members of the ensemble forecasts had either different forecast positions of the cyclone, central pressure, timing of cyclone landfall, or some combination of these factors. The large ensemble spread seen in Fig. 2a around the northern (i.e., northern Alaska) and eastern edge of the figure is an artifact of the EnKF boundary perturbation method (Torn et al. 2006) and should be ignored as it is not involved with the cyclone itself. The spread of the 24-h response function in this case is 6.35 hPa. The ensemble sensitivity of the cyclone central pressure to the initial sea level pressure field shows significantly high values in the vicinity of the incipient cyclone as indicated by the black arrow in Fig. 2b. Values greater than  $1.2 \text{ hPa hPa}^{-1}$  are in a broad region at the cyclone and north of it, with a maximum of  $1.6 \text{ hPa hPa}^{-1}$  immediately west-southwest of the center of the incipient cyclone. Significant regions of sensitivity are also found to the south of the cyclone near a surface

high and offshore of Southern California. This means that changes to the initial sea level pressure field both at the incipient cyclone itself and at the high to the south and along the southern west coast are all related to the forecast of the deepening cyclone.

The large ensemble spread in the vicinity of the forecast cyclone in Fig. 2a indicates that this storm has low predictability, as we have defined it for this study. The large ensemble sensitivity in Fig. 2b indicates that there was strong potential for perturbation growth in this case, so it is possible to surmise that perturbation growth was a significant factor in the low predictability. In the next section, we examine whether there are common synoptic features among landfalling cyclones with low or high predictability (both intrinsic and actual), such as deepening rate and storm track as seen in this example.

## b. Climatology of predictability

### 1) DEEPENING RATE

Maximum ensemble sensitivity and ensemble response function spread as a function of cyclone deepening rate are given in Fig. 3. In Fig. 3a, there is considerable variability of ensemble response function spread for deepening cyclones (data points to the left of the dashed black line), but most of the cyclones that are decaying exhibit smaller ensemble spread. The least squares fit line (blue dashed line in Fig. 3a) has a negative slope, meaning ensemble spread is larger for negative deepening rates (i.e., storms that deepen over 24 h). This

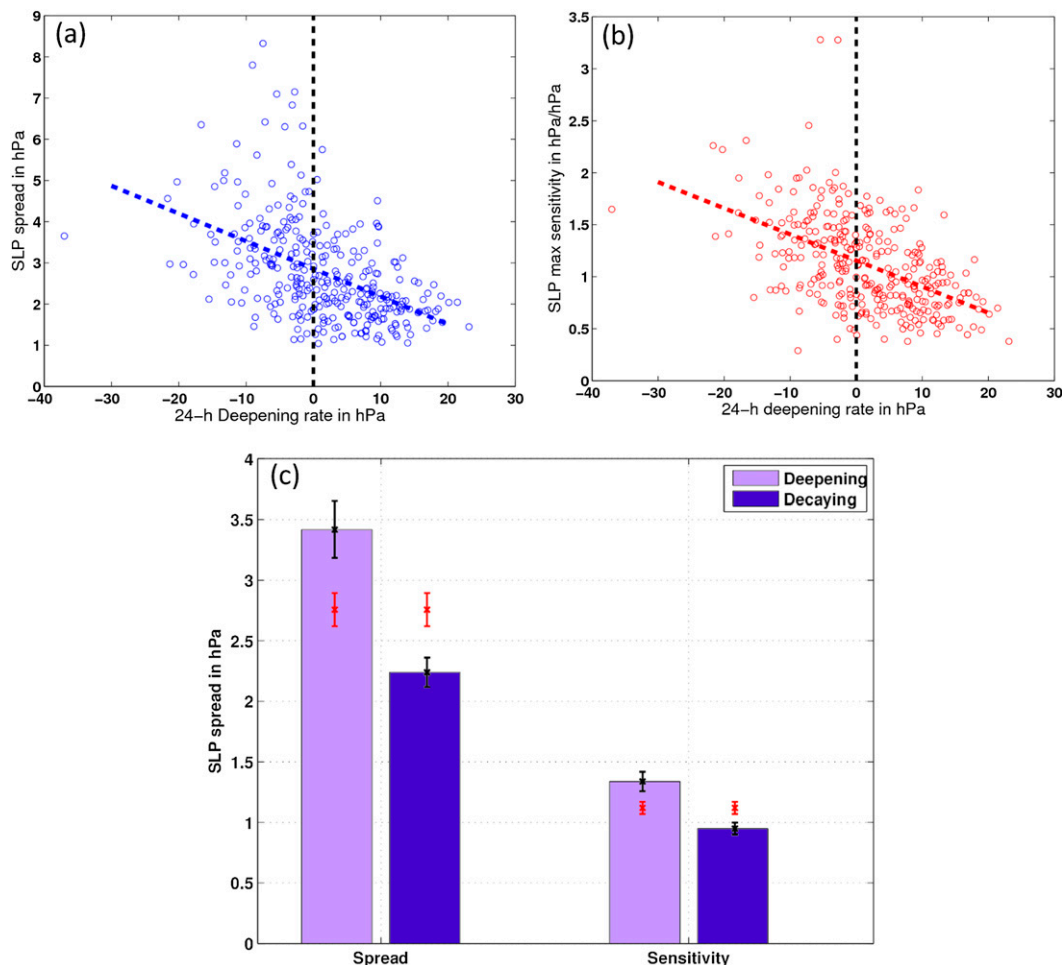


FIG. 3. Ensemble spread and ensemble sensitivity as a function of cyclone deepening rate. (a) Deepening rate [hPa (24 h)<sup>-1</sup>] vs ensemble spread (hPa) with a least squares fit line shown in dashed blue and the zero line for deepening rate in dashed black. (b) Deepening rate [hPa (24 h)<sup>-1</sup>] vs ensemble sensitivity (hPa hPa<sup>-1</sup>) with a least squares fit line shown in dashed red and the zero line for deepening rate in dashed black. (c) (left) Average ensemble spread and (right) average ensemble sensitivity in hPa for storms that are deepening (light purple) and for storms that are decaying (dark purple) over a 24-h forecast period. The 95% confidence intervals for each category are shown with the black error bars, and confidence intervals for the whole dataset set are shown with red error bars.

line passes the confidence test that the slope is significantly different from zero at 95% confidence. The left-hand side of Fig. 3c more clearly shows that deepening storms exhibit significantly more ensemble spread (and therefore less predictability) than decaying cyclones since the average ensemble spread for deepening storms is just under 3.5 hPa compared to 2.3 hPa for decaying storms and the 95% confidence interval for deepening storms is outside the interval for the entire dataset. The same relationship holds for ensemble sensitivity. The right-hand side of Fig. 3c indicates that deepening storms have higher ensemble sensitivity than decaying storms on average.

This result that larger response function spread and ensemble sensitivity tend to be associated with deepening cyclones is somewhat expected. If cyclones are viewed

as perturbations from the mean flow as in Langland et al. (1995), then it is reasonable to expect such growing perturbations (the deepening cyclones) to diverge throughout the forecast. Since large adjoint sensitivity likely accompanies large ensemble sensitivity (discussed in Ancell and Hakim 2007), it is not difficult to see that ensemble sensitivity is associated with large response function spread. On the contrary, decaying cyclones are likely converging back to the mean flow, producing less spread in the presence of smaller sensitivity magnitudes.

## 2) STORM TRACK

Average maximum spread and average maximum sensitivity are compared for storms tracking from different directions in Fig. 4a. All storms that come from

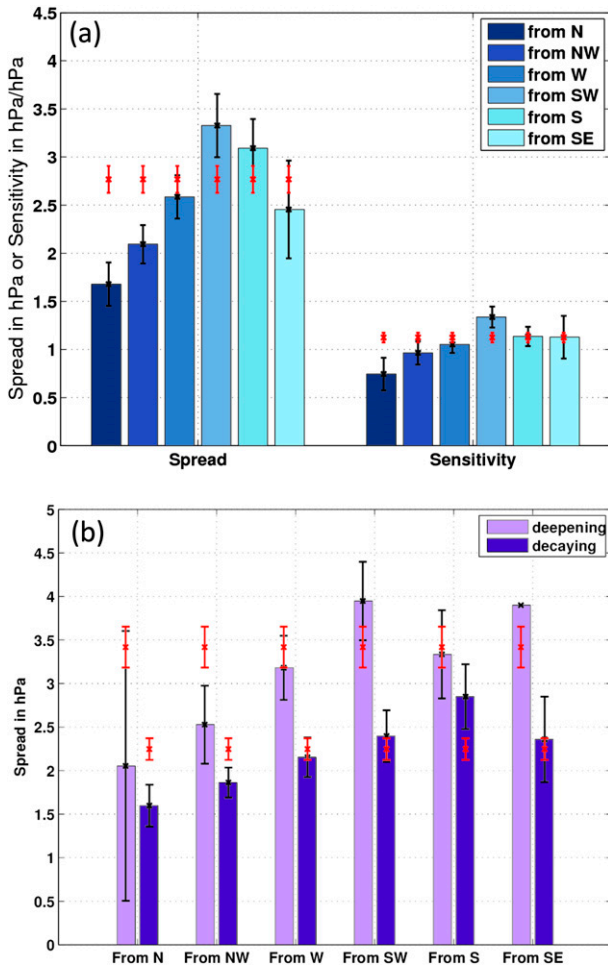


FIG. 4. (a) (left) Average maximum ensemble variance and (right) average maximum ensemble sensitivity for storms that track from different directions over the 24-h forecast period. The 95% confidence intervals are also indicated for each category in black and for the whole dataset in red. (b) Average maximum ensemble spread for storms in each storm track separated by deepening rate with deepening cyclones show in light purple and decaying cyclones in dark purple. The 95% confidence intervals are also indicated for each category in black and for the whole dataset in red. See Table 1 for the number of cyclones in each category.

within  $\pm 22.5^\circ$  of a particular direction (i.e., the southwest) are grouped in that direction. Storms that track from the southwest and south exhibit the largest response function spread and the highest sensitivity, while storms that track from the north and northwest have the smallest spread and lowest sensitivity. The response function spread for storms further partitioned into deepening and decaying storms for each storm track is shown in Fig. 4b. For all direction categories, deepening storms exhibit higher spread than decaying storms. However, there were very few deepening storms from the north and from the southeast (see Table 1), so that

comparisons with these categories are not possible. These results characterizing the predictability of cyclones from different directions can be explained in terms of deepening rates. In Table 1, the number of storms and the average deepening rate for each category is shown. Deepening storms from the south and southwest have larger mean deepening rates compared to deepening storms from the other directions [cf.  $-7.46 \text{ hPa (24 h)}^{-1}$  and  $-7.29 \text{ hPa (24 h)}^{-1}$  for the south and southwest to  $-5.86 \text{ hPa (24 h)}^{-1}$  for the west], and decaying storms from the north and northwest have the largest filling rates compared to decaying storms from other directions. Therefore, the differences between the response function spread for each storm direction shown in Fig. 4a is strongly related to differences in deepening rates for storms tracking from those different directions.

However, when comparing only deepening storms from the southwest to only deepening storms from the northwest, the southwest storms exhibit ensemble spread that is larger than the mean of all deepening storms, while the deepening storms from the northwest exhibit ensemble spread that is smaller than the mean of all deepening storms. This indicates that deepening storms that track from the southwest are less predictable than deepening storms that track from the northwest. When comparing decaying storms of each storm track category, a similar result is found: the storms from the south and southwest have slightly larger spread compared to the mean of all decaying storms, and storms from the north and northwest have lower spread than the mean of all decaying storms. Similar results are found when examining maximum ensemble sensitivity with the exception that sensitivities are not significantly different from the mean for decaying storms that track from any direction except the north and northwest (not shown).

These results, for which ensemble sensitivity and spread are largest for storms tracking from the southwest and smallest for storms tracking from the northwest, are consistent with those found in McMurdie and Casola (2009). In that study, observed sea level pressure forecast errors along the west coast of North America were compared for four different upper-level flow regimes. They found that the errors were largest when the upper-level flow was classified as a Rockies Ridge and small for the Alaska Ridge regime. The Rockies Ridge is characterized by zonal flow across the Pacific turning southwesterly just offshore of the North American coast and the Alaska Ridge is characterized by northwesterly flow offshore of the west coast.

With these striking differences between deepening storms tracking from the southwest compared to deepening storms tracking from the northwest, it's natural to

TABLE 1. Number and mean deepening rate [ $\text{hPa (24 h)}^{-1}$ ] for storms tracking from different directions.

| Storm direction | Deepening storms—Total No. | Deepening storms—Mean deepening rate | Decaying storms—Total No. | Decaying storms—Mean deepening rate |
|-----------------|----------------------------|--------------------------------------|---------------------------|-------------------------------------|
| N               | 3                          | -2.88                                | 14                        | 9.53                                |
| NW              | 16                         | -4.25                                | 30                        | 8.41                                |
| W               | 35                         | -5.86                                | 50                        | 7.01                                |
| SW              | 56                         | -7.29                                | 44                        | 7.31                                |
| S               | 30                         | -7.46                                | 30                        | 6.68                                |
| SE              | 1                          | -7.54                                | 15                        | 9.77                                |

wonder if there are substantial physical differences between storms taking different tracks in this region. We hypothesize that the southwest-tracking storms have lower intrinsic predictability than other storms because these storms are often dynamically active. Storms taking this track are most likely associated with amplifying upper-level short waves on the eastern side of an upper-level long-wave trough. This region would be characterized by large-scale upward vertical motion and is the favorable region for development. The strongest, most destructive wind events in the Pacific Northwest track from the southwest when they make landfall (Mass and Dotson 2010). Storms tracking from the northwest, on the other hand, would most likely be on the western side of an upper-level long-wave trough and in a region that is not as favorable for development.

### 3) STORM SPEED

In Fig. 5, ensemble response function spread and maximum ensemble sensitivity are compared to storm speed. For both spread and sensitivity, there is a slight increasing trend with increasing storm speed, but there is considerable variability around this trend, especially for ensemble spread. However, both least squares fit trend lines are significantly different from zero at the 95% confidence level. When the storms are placed into two speed categories (greater than or less than  $10 \text{ m s}^{-1}$ ), the faster storms exhibit larger spread and higher sensitivity than the slower storms (Fig. 5b) at 95% confidence. This suggests faster storms are both less predictable and possess larger intrinsic unpredictability than slower storms.

### 4) LATITUDE AT LANDFALL

In Fig. 6, the average ensemble spread and average maximum sensitivity are examined for storms partitioned by their latitude at landfall in  $5^\circ$  latitude bins. The storms that end within the  $50^\circ$ – $55^\circ\text{N}$  latitude band exhibit the largest spread and maximum sensitivity compared to the other latitude bands, and storms that end south of  $40^\circ\text{N}$  exhibit the least spread and sensitivity. Both of these are distinguishably different from the

average spread and sensitivity for the whole dataset. The average maximum sensitivity is further partitioned into deepening and decaying categories and is shown in Fig. 6b. Within each latitude band, deepening storms exhibit significantly higher ensemble sensitivity than decaying storms, as in our earlier results, except for storms ending south of  $40^\circ\text{N}$ . In this category, both deepening and decaying storms have similar average ensemble sensitivity. This is not due to unequal number of storms within the deepening (27 storms, see Table 2) and decaying (37 storms) groups. However, the deepening rates are not as different between deepening and decaying storms [ $-5.76 \text{ hPa (24 h)}^{-1}$  vs  $6.25 \text{ hPa (24 h)}^{-1}$  for deepening and decaying cyclones that end at  $40^\circ\text{N}$ , respectively, see Table 2] as in other latitude bands, such as  $50^\circ$ – $55^\circ\text{N}$  [ $-7.87 \text{ hPa (24 h)}^{-1}$  for deepening storms vs  $7.51 \text{ hPa (24 h)}^{-1}$  for decaying storms, see Table 2]. When individual cases are examined, a majority of the storms that end south of  $40^\circ\text{N}$  (both deepening and decaying) are fairly weak, slow moving surface lows that sometimes become cutoff lows off the California coast with an equivalent barotropic structure. The low sensitivity and low spread results for the south of  $40^\circ\text{N}$  group indicate that this type of storm (i.e., more equivalent barotropic vs baroclinic) has relatively high predictability with respect to sea level pressure compared to storms ending in other latitude bands. Despite their weak surface lows, this type of storm can sometimes have significant impact on the California coast in terms of precipitation. Even though this study demonstrates high predictability with respect to sea level pressure, there may be low predictability with respect to precipitation distribution and intensity.

Ensemble spread is larger for deepening cyclones than decaying cyclones for all latitude bands, including those storms that end south of  $40^\circ\text{N}$  (Fig. 6c). This reveals a very interesting property of the southernmost cyclones in the domain: deepening storms are less predictable than decaying storms even though the intrinsic predictability of deepening and decaying storms is roughly the same. This suggests through Eq. (2) that larger initial-time spread is responsible for the reduced predictability

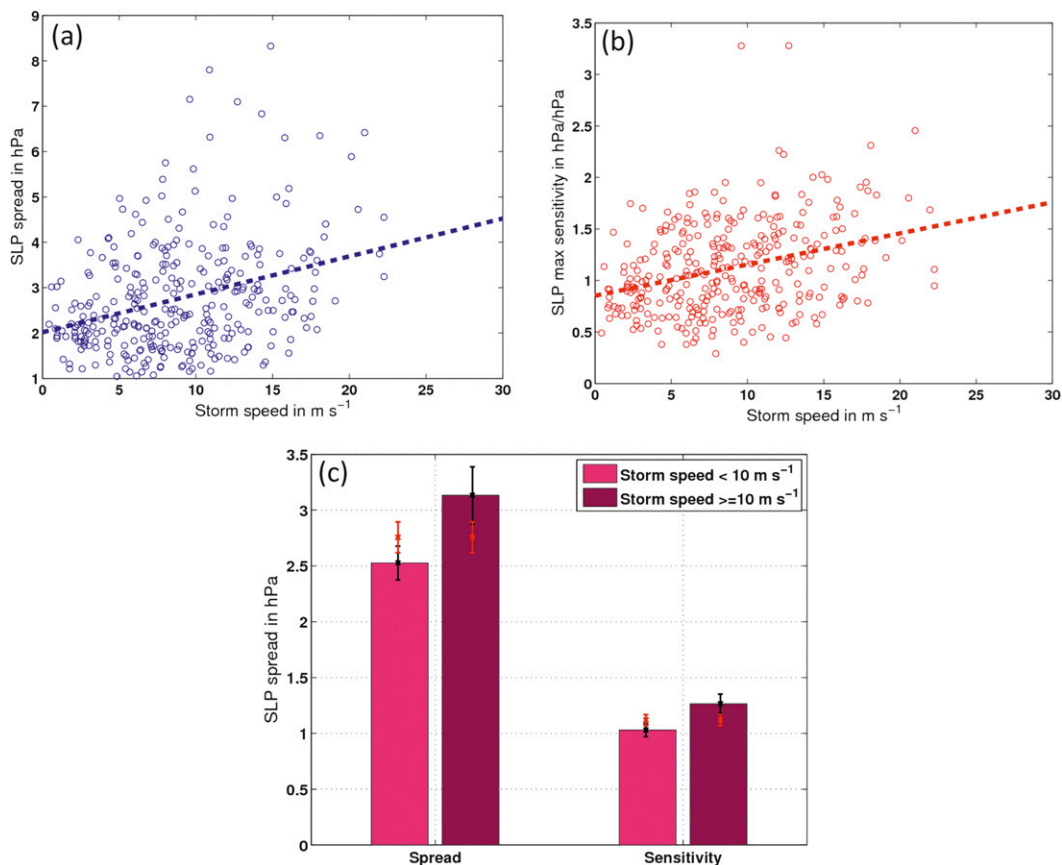


FIG. 5. Maximum ensemble spread and sensitivity as a function of storm speed. (a) Ensemble spread and storm speed ( $\text{m s}^{-1}$ ) with least squares fit line in blue. (b) Ensemble sensitivity and storm speed ( $\text{m s}^{-1}$ ) with least squares fit line in red. (c) (left) Average maximum ensemble spread and (right) average maximum ensemble sensitivity for storms speeds less than  $10 \text{ m s}^{-1}$  (light pink) and storm speeds greater than  $10 \text{ m s}^{-1}$  (dark pink). The 95% confidence intervals for each category are given in black and for the entire dataset are given in red.

of the deepening cyclones compared to decaying cyclones ending south of  $40^{\circ}\text{N}$ . The initial spread of sea level pressure was examined for all decaying and deepening cases ending south of  $40^{\circ}\text{N}$ . It was found that the deepening storms had an average initial spread of 1.85 hPa and the decaying storms had an average initial spread of 1.6 hPa. This difference is significant at the 87.5% confidence level confirming that the reduced predictability of the deepening cyclones was partly due to larger initial-time spread. The initial-time spread of other fields, such as 500-hPa heights or 850-hPa temperatures, were not examined.

##### 5) OBSERVATIONAL CONTEXT

The results presented above pertain to the “model world.” In this context, predictability is defined in terms of the model ensemble spread at the end of the forecast period (24 h) and not in terms of observed forecast error. However, it is worth establishing a relationship of our

measure of predictability to the more traditional measure of predictability where the value of a forecast parameter is compared to an observed value of the same parameter. Thus, to test the applicability of our definition, 24-h forecast errors of the mean sea level pressure response function were computed for each cyclone. Forecast error was defined by the difference between the 24-h ensemble mean response function and the 0-h analyzed response function. The maximum ensemble sensitivity and ensemble spread for cases where the forecast errors were greater than 3 hPa are compared to the maximum ensemble sensitivity and ensemble spread for cases where the forecast errors were less than 3 hPa and are shown in Fig. 7a. The results show that the observed forecast error is larger than the mean forecast error for cyclones with large ensemble spread and the observed forecast error is smaller than the mean error for cyclones with small ensemble spread. The same was true for ensemble sensitivity. Alternatively, the average

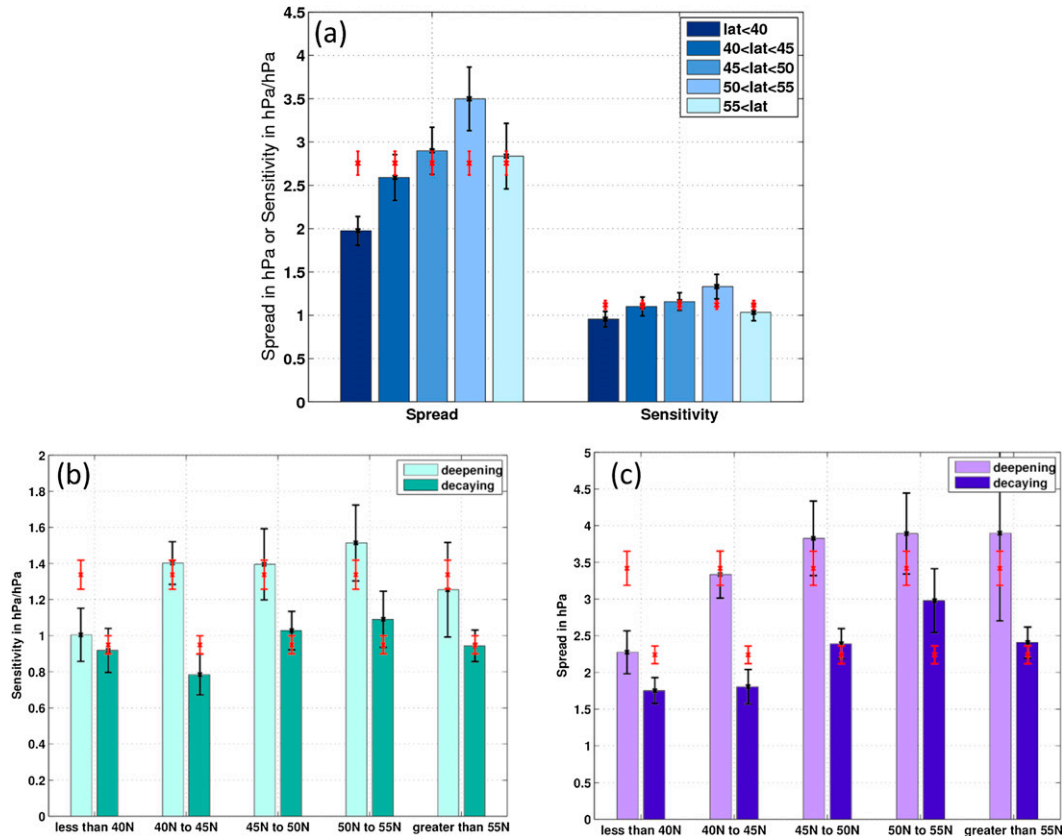


FIG. 6. (a) (left) Average maximum ensemble spread and (right) average maximum ensemble sensitivity for storms that end within various latitude bands at 24-h forecast time. (b) Average maximum ensemble sensitivity for deepening (light cyan) and decaying (dark cyan) for storms that end within various latitude bands at 24-h forecast time. (c) Average spread for deepening (light purple) and decaying storms (dark purple) that end in various latitude bands at 24-h forecast time. In each panel, the 95% confidence intervals are indicated by error bars for each category in black and for all, deepening, or decaying cases in red.

forecast error was calculated for cases with large ensemble spread ( $>3$  hPa), small ensemble spread ( $<2$  hPa), high sensitivity ( $>1.6$  hPa hPa $^{-1}$ ), and low sensitivity ( $<1.2$  hPa hPa $^{-1}$ ) and are shown in Fig. 7b. The average forecast error is larger than the mean for cases with large spread and lower than the mean for cases with small spread. However, the average forecast error was not significantly different from the mean for cases of high and low sensitivity. This implies that the definition of predictability in terms of modeled ensemble spread is appropriate and applies generally to forecast error as might be expected with a calibrated ensemble spread-skill relationship (Houtekamer et al. 2005). On the contrary, ensemble sensitivity is not necessarily an indication of forecast accuracy for all cases. Several factors could be contributing to this. For example, if a storm exhibits relatively large initial-condition sensitivity yet is well analyzed at the initial time, the forecast may be somewhat accurate despite the lack of intrinsic

predictability as indicated by large sensitivity. In addition, if forecasts were made for longer lead times (i.e., 48 or 72 h), it is likely that more cases with high initial sensitivity would exhibit larger forecast errors when there is sufficient time for the forecast spread to grow. This will be explored further in the next section.

TABLE 2. Mean deepening rates [hPa (24 h) $^{-1}$ ] and total number of storms ending within different latitude bands.

| Lat at landfall               | Deepening total No. | Deepening mean deepening rate | Decaying total No. | Decaying mean deepening rate |
|-------------------------------|---------------------|-------------------------------|--------------------|------------------------------|
| $<40^{\circ}$ N               | 27                  | -5.76                         | 37                 | 6.25                         |
| $40^{\circ}$ - $45^{\circ}$ N | 38                  | -6.21                         | 40                 | 8.08                         |
| $45^{\circ}$ - $50^{\circ}$ N | 24                  | -6.11                         | 44                 | 7.89                         |
| $50^{\circ}$ - $55^{\circ}$ N | 38                  | -7.87                         | 31                 | 7.51                         |
| $>55^{\circ}$ N               | 15                  | -5.69                         | 37                 | 8.41                         |

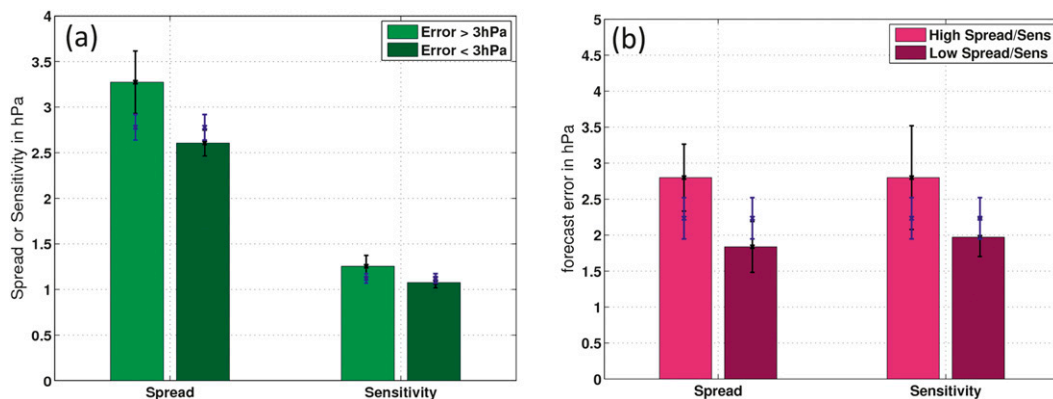


FIG. 7. (a) The average spread and sensitivity for cyclones with 24-h forecast errors greater than 3 hPa (light green) and 24-h forecast errors less than 3 hPa (dark green) at the location of the cyclone at landfall (i.e., at the location of the response function). (b) The average forecast error for cyclones with ensemble spread greater than 3 hPa and ensemble sensitivity greater than  $1.6 \text{ hPa hPa}^{-1}$  (light pink) and for cyclones with ensemble spread less than 2 hPa and ensemble sensitivity less than  $1.2 \text{ hPa hPa}^{-1}$  (dark pink). The 95% confidence intervals are indicated by error bars for each category in black and for all cases in blue.

### c. Composites

When ensemble sensitivity is large, there is a large potential for perturbation growth over the course of the forecast period. Therefore, one would expect that ensemble spread would also be higher for cases with large initial-condition sensitivity. In Fig. 8, ensemble response function spread versus maximum ensemble sensitivity for all the cyclones included in the study is shown. Indeed, increased ensemble spread is related to larger ensemble sensitivity. However, there is considerable variability in ensemble spread, especially at higher sensitivities. In this section we explore this variability to understand whether certain flow situations that produce cyclones (e.g., frontal waves, comma clouds) are related to any of the following four categories: large spread/high sensitivity, large spread/low sensitivity, small spread/high sensitivity, and small spread/low sensitivity.

#### 1) LARGE ENSEMBLE SPREAD AND HIGH ENSEMBLE SENSITIVITY

Here we calculate sea level pressure and 500-hPa height composites and anomalies from the Global Forecast System (GFS)  $0.5^\circ$  analyses for storms that exhibit ensemble response function spread greater than 3 hPa and maximum ensemble initial-condition sensitivity greater than  $1.6 \text{ hPa hPa}^{-1}$ . The anomalies of sea level pressure and 500-hPa heights were computed by subtracting the composites from a climatology computed from the same GFS grids for the period October 2008/March 2009 and October 2009/March 2010, a two cold-season climatology. There were 44 24-h forecasts of cyclones, out of 331, that met these criteria. These

cyclones have large intrinsic potential for perturbation growth and result in large ensemble spread (i.e., low predictability).

The composite 500-hPa heights and locations of the cyclones are given for the initial time in Fig. 9a and 24-h forecast time in Fig. 9b. At the initial time, the locations of the cyclones are well spread out across the mid-Pacific with a majority of them within the  $40^\circ$ – $50^\circ\text{N}$  latitude band. The initial 500-hPa height field exhibits a broad upper-level trough at about  $145^\circ\text{W}$  with upstream ridging. Since there is a large spread of initial positions longitudinally, the composite upper-level trough associated with these cases is weaker and broader than

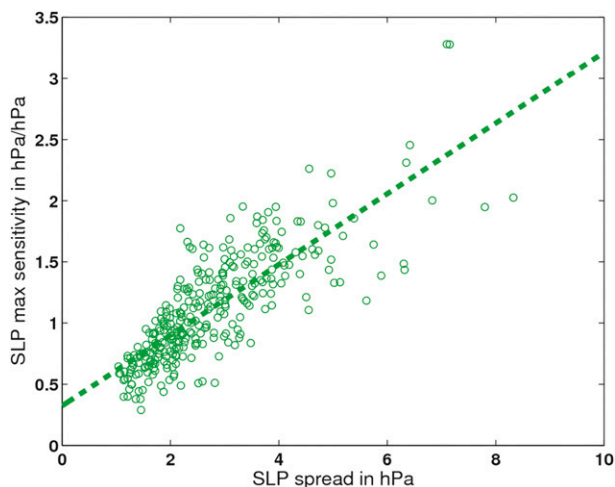


FIG. 8. Maximum ensemble spread vs maximum sensitivity for all cases during the 2008–10 winter seasons. The dashed green line represents the line of least squares fit.

## Large Ensemble Spread and High Maximum Ensemble Sensitivity

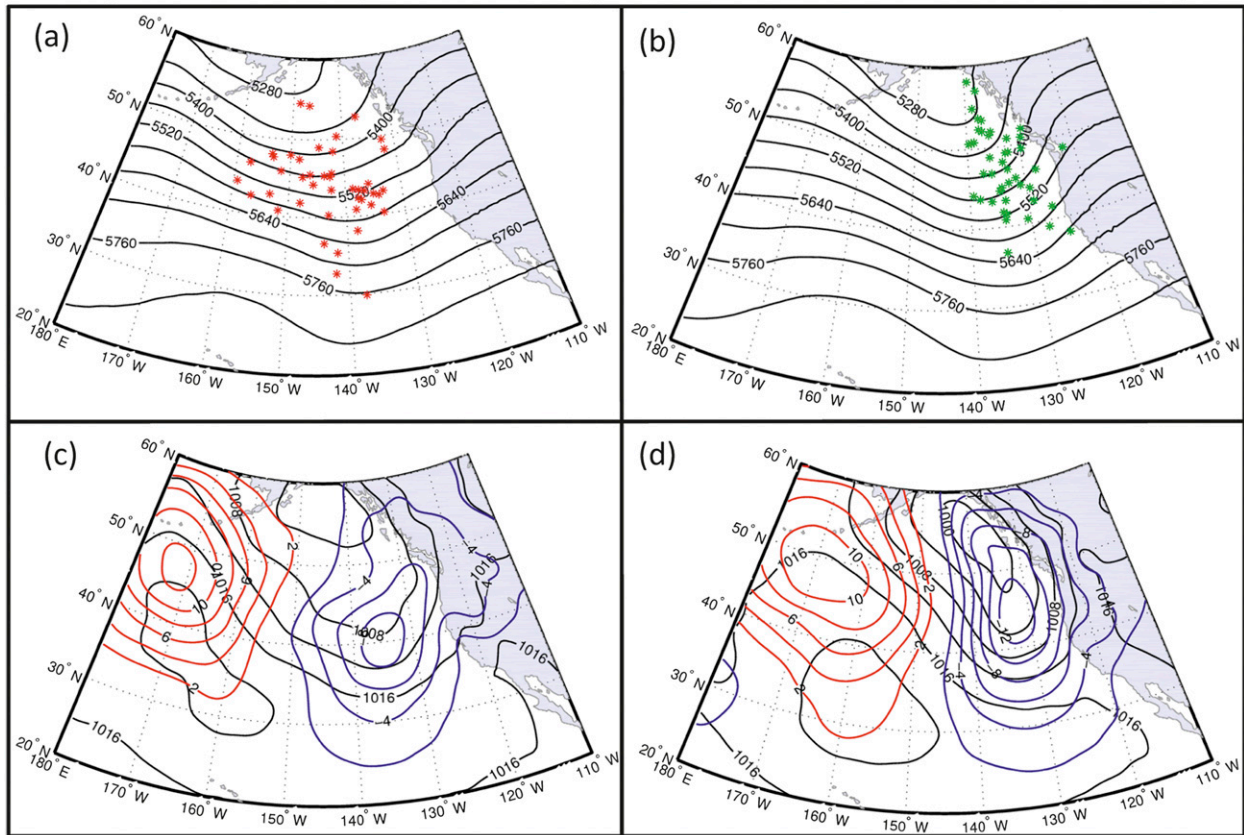


FIG. 9. Composite heights and sea level pressure for cases with large ensemble spread and high maximum ensemble sensitivity. (a) Composite 500-hPa heights (contour interval 60 m) at the initialization time (F00) with the initial location of each cyclone indicated with red stars (\*). (b) Composite 500-hPa heights at the 24-h forecast time with the final position of each cyclone indicated with green stars (\*). (c) Composite sea level pressure (every 4 hPa) for the initialization time and the difference between the composite field and the 2008–10 climatology given in red (positive) and blue (negative) contours (every 1 hPa). (d) As in (c), but for the 24-h forecast time. Total number of cases for this composite = 44.

would be seen for individual cyclones. At the forecast time (Fig. 9b), the upper-level trough has sharpened and deepened and is situated right offshore.

The composite sea level pressure fields for the initial and final times are given in Figs. 9c and 9d with the anomalies given in red (positive) and blue (negative) contours. At the initial time, the composite sea level pressure field shows a broad offshore surface low of 1004 hPa centered in the Gulf of Alaska, with the center of the sea level pressure anomaly of  $-8$  hPa at  $41^{\circ}\text{N}$  and  $135^{\circ}\text{W}$ . Upstream there is a high pressure anomaly of 11 hPa at about  $170^{\circ}\text{W}$ . At the 24-h forecast time, the surface low in the Gulf of Alaska has deepened and anomalous sea level pressure center is now  $-12$  hPa located at  $43^{\circ}\text{N}$  and  $132^{\circ}\text{W}$ . A histogram of storm tracks for these cases show that over half of the cases track from the southwest, with most of the rest from the west and south directions (not shown). The deepening rates

for these storms range from  $-20$  to  $8$  hPa  $(24\text{ h})^{-1}$  and averages  $-6.0$  hPa  $(24\text{ h})^{-1}$  (not shown). When the cases are limited to storms that end within a box  $40^{\circ}\text{--}50^{\circ}\text{N}$  and  $140^{\circ}\text{--}130^{\circ}\text{W}$ , the composite sea level pressure and 500-hPa fields show even a larger amplification of the upper-level trough and stronger deepening of the surface cyclone over the 24 h (not shown). These composites all indicate that, on average, cases with large spread and high sensitivity are deepening cyclones that track from the southwest, west, and south.

### 2) LARGE ENSEMBLE SPREAD AND LOW ENSEMBLE SENSITIVITY

Composite 500-hPa heights and sea level pressure are shown in Fig. 10 for storms with ensemble response function spread greater than 3 hPa and maximum initial-condition sensitivity less than  $1.2$  hPa hPa $^{-1}$ . There were a total of 42 cases that fit these criteria. These cyclones

## Large Ensemble Spread and Low Maximum Ensemble Sensitivity

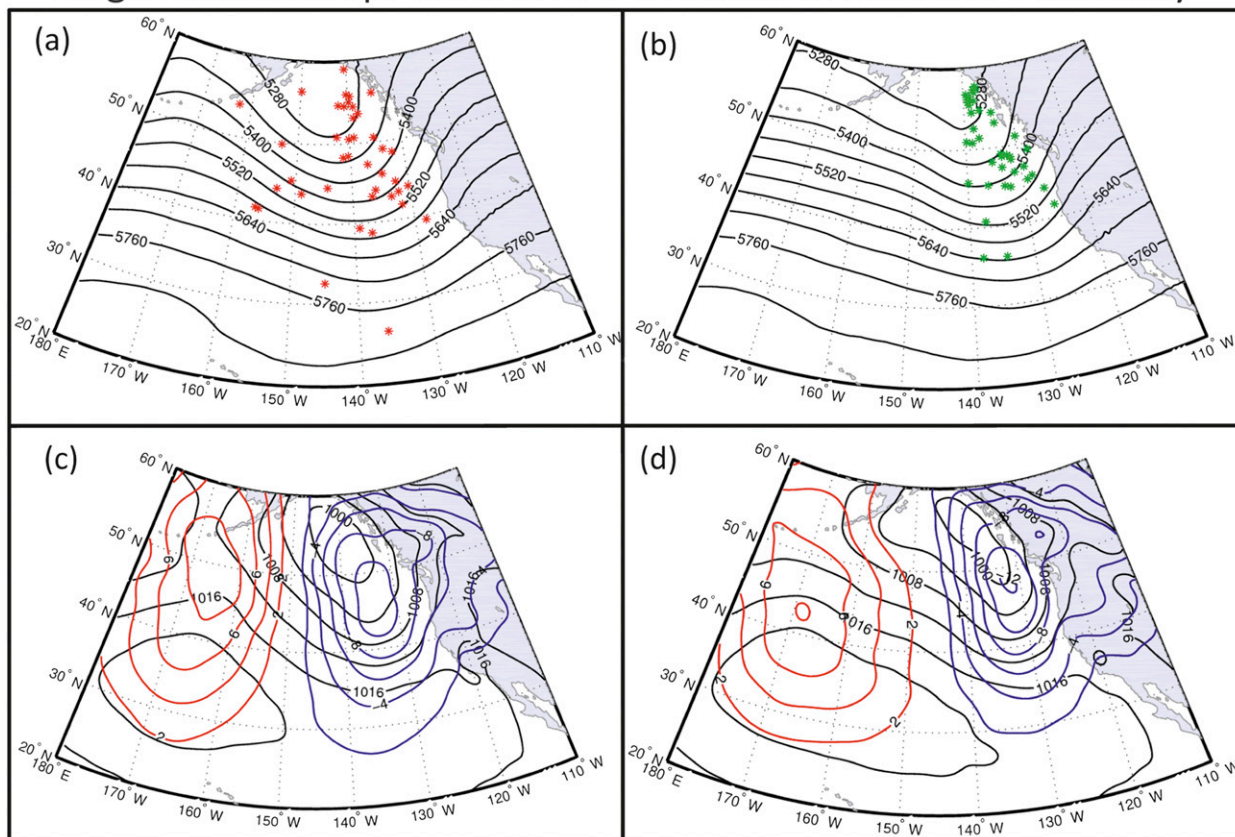


FIG. 10. As in Fig. 9, but for cases with large ensemble spread and low maximum ensemble sensitivity. Total number of cases for this composite = 42.

are those for which small intrinsic potential for perturbation growth exists, but still results in large ensemble spread.

In contrast to the previous case, at the initial time, these storms are associated with a significant upper-level trough (Fig. 10a) and a deeper composite surface low of 1000 hPa (Fig. 10c). The initial position of these cyclones also are scattered across the North Pacific, as in the previous case, so that the upper-level trough and surface low are probably more intense for individual cyclones than seen in the composites. At the 24-h forecast time, the upper-level trough has amplified slightly and the surface low has also deepened somewhat. The location of the maximum sea level pressure anomaly of  $-12$  hPa is at  $48^{\circ}\text{N}$  and  $132^{\circ}\text{W}$  and is farther north than the previous case (Fig. 9). The range of deepening rates for this category is quite large, from  $-16$  to  $16$  hPa  $(24\text{ h})^{-1}$  with an average of  $1.9$  hPa  $(24\text{ h})^{-1}$ . The majority of the storms track from the west, with quite a few from the southwest and south, similar to the large spread/high sensitivity cases shown in the previous section.

The composites appear to show that these large spread/low sensitivity cases are already mature or deep cyclones

at the beginning of the forecast cycle. Their low predictability (i.e., high ensemble spread) is most likely due to large initial-time spread that does not grow much over the 24 h (since the sensitivity is low). To explore this, the initial-time spread fields of sea level pressure were examined. It was found that the mean initial-time spread for large spread/low sensitivity cases was  $3.3$  hPa compared to  $2.96$  hPa for the mean initial-time spread for large spread/high sensitivity cases of the previous section. The difference between these two means is significant at the 90% level. At the 24-h forecast time, this ensemble spread did not grow much with a mean 24-h spread of only  $3.5$  hPa for this category compared to a mean of  $4.5$  for the large spread/high sensitivity case. Therefore, it is likely that reduced predictability for large spread/low sensitivity cases are primarily due to larger initial-condition spread rather than perturbation growth.

To further illustrate the differences between these two categories, the initial-time and forecast-time ensemble spread is shown for two representative cases: 0600 UTC 31 December 2009 with a large ensemble spread and low

### Ensemble Spread at Initial and Forecast Times

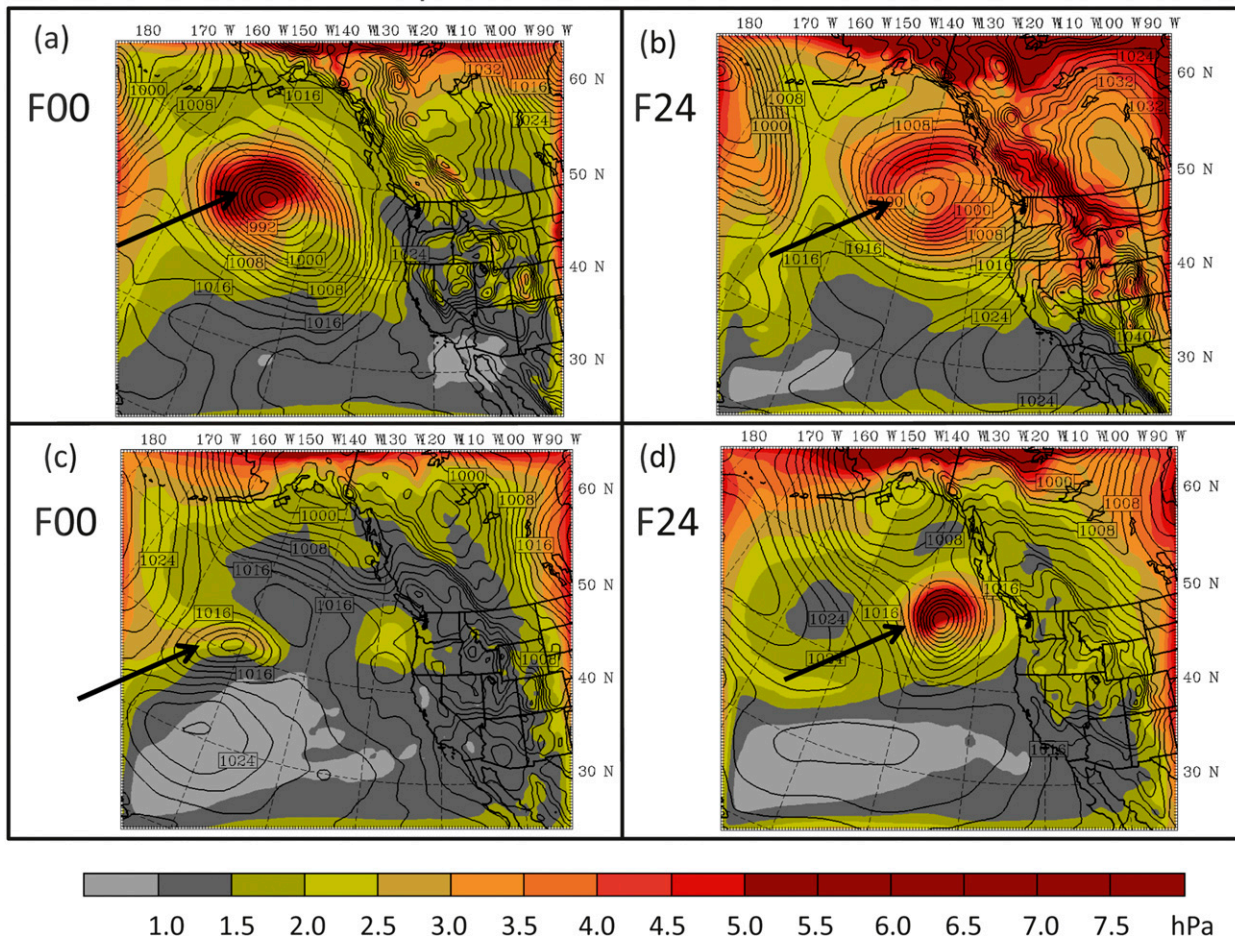


FIG. 11. Comparison of initial-time spread and forecast ensemble spread for two cases. The 0600 UTC 31 Dec 2009 case with large initial-time spread, small initial-time sensitivity, and large final-time spread: (a) initial-time spread (F00) and (b) final-time spread (F24). The 1800 UTC 5 Oct 2008 case with small initial-time spread, large initial-time sensitivity, and large final-time spread: (c) initial-time spread (F00) and (d) final-time spread (F24). Black arrows point to storm and its ensemble spread.

ensemble sensitivity case, and 1800 UTC 5 October 2008 with a large ensemble spread and high ensemble sensitivity case. The 31 December 2009 case occurred during a time when one of the data sources, cloud track winds, were missing from the archives. Subsequently, the data assimilation system appears to have had less success in accurately depicting the location of the mature cyclone and large initial-time spread over a large area as evident in Fig. 11a. However, the ensemble sensitivity is rather low,  $0.6 \text{ hPa hPa}^{-1}$ , and the ensemble spread remains the same or slightly decreases over the 24-h period (Fig. 11b). The 5 October 2008 case, on the other hand, exhibits much smaller initial-time spread (Fig. 11c) yet has a much larger ensemble sensitivity of  $1.7 \text{ hPa hPa}^{-1}$ . By 24-h the ensemble spread has grown substantially to a maximum over  $5 \text{ hPa}$  (Fig. 11d).

Note that the 31 December 2009 case and other storms that occurred during the cloud track wind data outage (14 December 2009–4 January 2010) are not included in any of the statistics or composites in the analysis presented here. This assures consistency of data availability for all cases. However, the 31 December 2009 case is used here to illustrate that lack of data in critical regions can have a strong effect on subsequent forecasts even when the intrinsic predictability is large.

#### 3) SMALL ENSEMBLE SPREAD AND HIGH ENSEMBLE SENSITIVITY

This category includes storms with ensemble spread less than  $2 \text{ hPa}$  and maximum initial-condition sensitivity to sea level pressure greater than  $1.2 \text{ hPa hPa}^{-1}$ . The total number of cases is 14. If the maximum initial-condition

## Small Ensemble Spread and High Maximum Ensemble Sensitivity

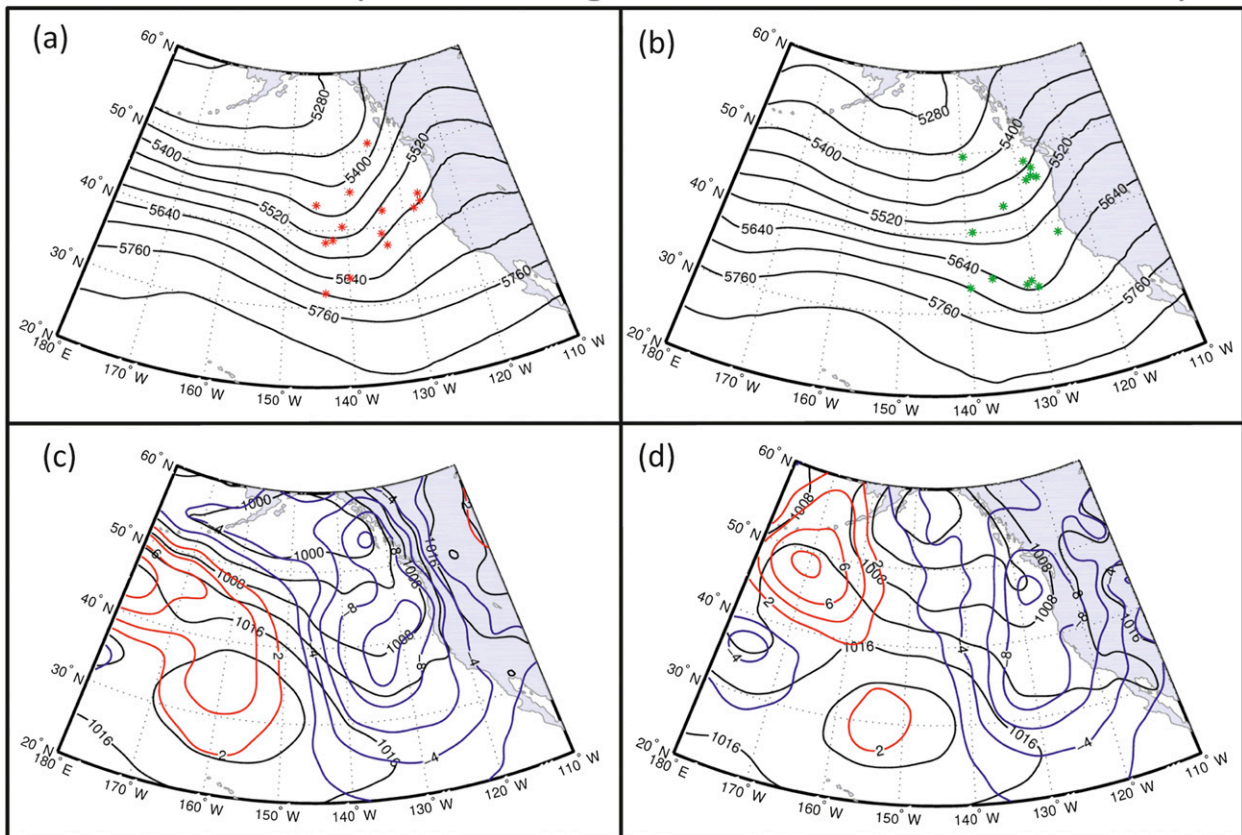


FIG. 12. As in Fig. 9, but for cases with small ensemble spread and high maximum ensemble sensitivity. Total number of cases for this composite = 14.

sensitivity was required to be greater than  $1.6 \text{ hPa hPa}^{-1}$ , as in the first case (section 1 above), then there would only be four cases that fit the criteria. This particular category is relatively rare since high sensitivity usually produces perturbation growth and increases the likelihood of large ensemble spread at the forecast time. Nonetheless, these cases represent cyclones where high predictability occurred in the presence of low intrinsic predictability.

The composite 500-hPa heights at initial time show a modest upper-level trough situated offshore around  $140^\circ\text{W}$  and relatively zonal flow upstream (Fig. 12a). The sea level pressure composite has a low center in the Gulf of Alaska of 1000 hPa (Fig. 12c). By the 24-h forecast time, the composites show a significant weakening of both features indicating that, on average, these storms are decaying. This is confirmed in a histogram of deepening rates for these cases: the mean deepening rate is  $3.1 \text{ hPa (24 h)}^{-1}$ , and ranges from  $-4$  to  $8 \text{ hPa (24 h)}^{-1}$  (not shown). A histogram of storm directions reveals that there is no preferred direction for this group of storms. A third of the storms are from the northwest,

and third from the southwest and the rest are spread among the north, south, and west directions. In some regards, this group of storms is the success story of predictability in the region. They all exhibited the potential for growth with the relatively large initial-condition ensemble sensitivity but there was less uncertainty in the forecast, since the forecast ensemble spread is small. The composites show that weakening storms that have larger sensitivity are still forecasted relatively well.

#### 4) SMALL ENSEMBLE SPREAD AND LOW ENSEMBLE SENSITIVITY

This category includes storms that have ensemble spread less than 2 hPa and initial-condition ensemble sensitivity less than  $0.6 \text{ hPa hPa}^{-1}$ . There are 29 cases that fit these criteria. If the ensemble sensitivity was set higher at  $1.2 \text{ hPa hPa}^{-1}$ , such as in category 2 above, then there would be 89 cases. The results are essentially the same for both groups.

The composite 500-hPa heights and sea level pressure at initial and final times are shown in Fig. 13. At the initial

### Small Ensemble Spread and Low Maximum Ensemble Sensitivity

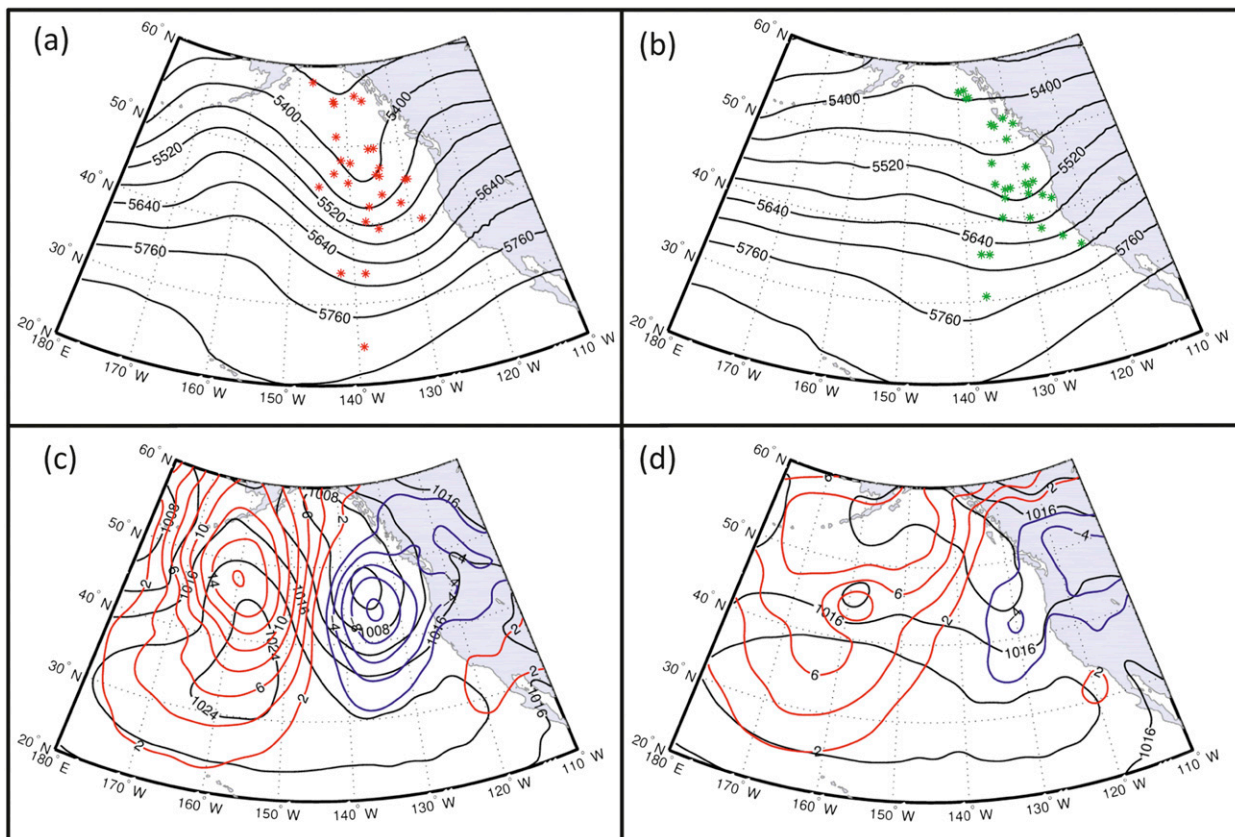


FIG. 13. As in Fig. 9, but for cases with small ensemble spread and low maximum ensemble sensitivity. Total number of cases for this composite = 29.

time, there is a significant upper-level trough (Fig. 13a) and 1004-hPa low pressure center offshore centered at approximately 45°N, 135°W. By the final forecast time, both these features have weakened considerably with the composite 500-hPa trough decreasing from 5400 to 5580 m and the composite surface low weakening from 1004 to 1012 hPa. The average deepening rate for this group is  $7.1 \text{ hPa (24 h)}^{-1}$ , and it ranges from  $-8$  to  $20 \text{ hPa (24 h)}^{-1}$ . This group clearly contains storms that weakened significantly as they approach the west coast and have the highest predictability.

#### 5. Summary and conclusions

In this study, we use a WRF EnKF to investigate the predictability, ensemble sensitivity, and spread characteristics of landfalling cyclones on the west coast of North America over two winter seasons (2008/09 and 2009/10). We define predictability in terms of ensemble spread of a storm's central sea level pressure at the final forecast time (24 h), where low predictability exhibits

large ensemble spread and high predictability exhibits small ensemble spread. Our primary results can be summarized as follows:

- Deepening storms and storms that track from the southwest have the highest ensemble spread and largest ensemble initial-condition sensitivity compared to decaying storms and storms that track from other directions.
- Storms that make landfall south of 40°N, which tend to be slow-moving storms tracking from the northwest that form cutoff lows off the coast of California, exhibit the highest predictability compared to storms ending north of 40°N regardless of whether they are deepening or decaying.
- Storms that have large ensemble spread and high ensemble initial-condition sensitivity are deepening cyclones that track primarily from the west, southwest, or south. The high initial-condition sensitivity is likely a significant contributor to the lower predictability of these cyclones.

- Storms that have large ensemble spread but low ensemble initial-condition sensitivity are mature cyclones at the initial time, exhibit a range of deepening rates and generally track from the west, southwest, or south. The low predictability of these cyclones is likely due to large initial-condition spread that does not grow much over the 24-h forecast period.
- Storms with small ensemble spread but high ensemble sensitivity are relatively rare, and are mostly weakening cyclones. They appear to be forecasted well despite the high initial-condition sensitivity, and likely represent the small number of cyclone cases where initial ensemble spread was not able to take advantage of the large potential for perturbation growth (as revealed by the large sensitivity field).
- Storms with small ensemble spread and low ensemble sensitivity are decaying cyclones with a deamplifying upper-level trough. These storms have the highest predictability.

In this study, we only examined a storm's predictability in terms of the cyclone's central sea level pressure. There are many other aspects of a cyclone that are important to forecast accurately such as precipitation distribution, precipitation intensity, temperature, and humidity. These other aspects may be more important than sea level pressure for some types of storm systems, such as the weak cutoff lows off the California coast. If these forecast aspects were used for the response function instead of the cyclones central pressure, then the results may be different than those found here. Nonetheless, it is likely that the results apply to some degree to these other aspects since they are dynamically linked to the parent cyclone. The precise relationship, however, can only be discovered through further study using different response functions.

The techniques used in this study can be applied to storms occurring in other locations, such as along the east coast of North America or Asia or approaching Europe. Future studies could explore whether deepening rate is found to be universally important to the predictability of all storms everywhere or unique to landfalling cyclones along the west coast of North America. It is likely that there would be regional differences in the cyclone features that are associated with low predictability since storms are typically at different stages of their life cycle in particular regions (i.e., storms are often at the initial stages along the east coast of North America and at their mature or decaying stages along the west coast of North America).

This study has revealed particular types of cyclones that possess low predictability as a result of a large dynamical potential for error growth, a situation that is

practically impossible to mitigate. However, certain situations were shown to produce relatively unpredictable cyclones as a result of large initial spread (and not a large potential for perturbation growth). In these cases, it is reasonable to expect that better data assimilation may improve forecasts of these cyclones since additional observations have the ability to reduce initial-time uncertainty. It is beyond the scope of this study to investigate how a modified observational network might improve forecasts of these cyclones, but such an examination is a logical next step in order to address the poor predictability of these specific cyclones identified here.

*Acknowledgments.* The authors thank Dr. Rolf Langland for discussions and support at the initial stages of this research. This study was partially funded by NRL Grant N00173-09-1-G024. The authors would also like to thank the Texas Tech High Performance Computing Center for their support of the computing resources required to perform the experiments in this study.

#### REFERENCES

- Ancell, B. C., 2013: Nonlinear characteristics of ensemble perturbation evolution and their application to forecasting high-impact events. *Wea. Forecasting*, in press.
- , and C. F. Mass, 2006: Structure, growth rates, and tangent linear accuracy of adjoint sensitivities with respect to horizontal and vertical resolution. *Mon. Wea. Rev.*, **134**, 2971–2988.
- , and G. J. Hakim, 2007: Comparing ensemble and adjoint sensitivity analysis with applications to observation targeting. *Mon. Wea. Rev.*, **135**, 4117–4134.
- , and L. A. McMurdie, 2013: Ensemble adaptive data assimilation techniques applied to land-falling North American cyclones. *Data Assimilation*, L. Xu and S. Park, Eds., Vol. 2, Springer, 555–576.
- Anderson, J. L., and S. L. Anderson, 1999: A Monte Carlo implementation of the nonlinear filtering problem to produce ensemble assimilations and forecasts. *Mon. Wea. Rev.*, **127**, 2741–2758.
- Badger, J., and B. J. Hoskins, 2001: Simple initial value problems and mechanisms for baroclinic growth. *J. Atmos. Sci.*, **58**, 38–49.
- Barker, D., and Coauthors, 2012: The Weather Research and Forecasting Model's Community Variational/Ensemble Data Assimilation System: WRFDA. *Bull. Amer. Meteor. Soc.*, **93**, 831–843.
- Chang, E. K. M., M. Zheng, and K. Raeder, 2013: Medium-range ensemble sensitivity analysis of two extreme Pacific extratropical cyclones. *Mon. Wea. Rev.*, **141**, 211–231.
- Charles, M. E., and B. A. Colle, 2009: Verification of extratropical cyclones within the NCEP operational models. Part I: Analysis errors and short-term NAM and GFS forecasts. *Wea. Forecasting*, **24**, 1173–1190.
- Chen, F., and J. Dudhia, 2001: Coupling an advanced land-surface/hydrology model with the Penn State/NCAR MM5 modeling system. Part I: Model description and implementation. *Mon. Wea. Rev.*, **129**, 569–585.

- Colle, B. A., and M. E. Charles, 2011: Spatial distribution and evolution of extratropical cyclone errors over North America and its adjacent oceans in the NCEP global forecast system model. *Wea. Forecasting*, **26**, 129–149.
- Dudhia, J., 1989: Numerical study of convection observed during the winter monsoon experiment using a mesoscale two-dimensional model. *J. Atmos. Sci.*, **46**, 3077–3107.
- Errico, R. M., 1997: What is an adjoint model? *Bull. Amer. Meteor. Soc.*, **78**, 2577–2591.
- Evensen, G., 1994: Sequential data assimilation with a nonlinear quasi-geostrophic model using Monte Carlo methods to forecast error statistics. *J. Geophys. Res.*, **99** (C5), 10143–10162.
- Gaspari, G., and S. E. Cohn, 1999: Construction of correlation functions in two and three dimensions. *Quart. J. Roy. Meteor. Soc.*, **125**, 723–757.
- Gelaro, R., R. Buizza, T. N. Palmer, and E. Klinker, 1998: Sensitivity analysis of forecast errors and the construction of optimal perturbations using singular vectors. *J. Atmos. Sci.*, **55**, 1012–1037.
- Gilmour, I., L. A. Smith, and R. Buizza, 2001: Linear regime duration: Is 24 hours a long time in synoptic weather forecasting? *J. Atmos. Sci.*, **58**, 3525–3539.
- Hakim, G. J., and R. D. Torn, 2008: Ensemble synoptic analysis. *Synoptic-Dynamic Meteorology and Weather Analysis and Forecasting: A Tribute to Fred Sanders*, Meteor. Monogr., No. 55, Amer. Meteor. Soc., 147–161.
- Hong, S.-Y., J. Dudhia, and S.-H. Chen, 2004: A revised approach to ice microphysical processes for the bulk parameterization of clouds and precipitation. *Mon. Wea. Rev.*, **132**, 103–120.
- Hoskins, B. J., R. Buizza, and J. Badger, 2000: The nature of singular vector growth and structure. *Quart. J. Roy. Meteor. Soc.*, **126**, 1565–1580.
- Houtekamer, P. L., H. L. Mitchell, G. Pellerin, M. Buehner, M. Charron, L. Spacek, and B. Hansen, 2005: Atmospheric data assimilation with an ensemble Kalman filter: Results with real observations. *Mon. Wea. Rev.*, **133**, 604–620.
- Janjic, Z. I., 1990: The step-mountain coordinate: Physical package. *Mon. Wea. Rev.*, **118**, 1429–1443.
- , 1996: The surface layer in the NCEP Eta Model. Preprints, *11th Conf. on Numerical Weather Prediction*, Norfolk, VA, Amer. Meteor. Soc., 354–355.
- , 2002: Nonsingular implementation of the Mellor–Yamada Level 2.5 scheme in the NCEP Meso model. NCEP Office Note 437, 61 pp.
- Kain, J. S., and J. M. Fritsch, 1990: A one-dimensional entraining/detraining plume model and its application in convective parameterization. *J. Atmos. Sci.*, **47**, 2784–2802.
- , and —, 1993: Convective parameterization for mesoscale models: The Kain–Fritsch scheme. *The Representation of Cumulus Convection in Numerical Models*, Meteor. Monogr., No. 24, Amer. Meteor. Soc., 165–170.
- Kalnay, E., 2002: *Atmospheric Modeling, Data Assimilation, and Predictability*. Cambridge University Press, 364 pp.
- Klinker, E., F. Rabier, and R. Gelaro, 1998: Estimation of key analysis errors using the adjoint technique. *Quart. J. Roy. Meteor. Soc.*, **124**, 1909–1933.
- Langland, R. H., R. L. Elsberry, and R. M. Errico, 1995: Evaluation of physical processes in an idealized extratropical cyclone using adjoint sensitivity. *Quart. J. Roy. Meteor. Soc.*, **121**, 1349–1386.
- Mass, C. F., and B. Dotson, 2010: Major extratropical cyclones of the northwest United States: Historical review, climatology, and synoptic environment. *Mon. Wea. Rev.*, **138**, 2499–2527.
- Matsueda, M., M. Kyouda, Z. Toth, H. L. Tanaka, and T. Tsuyuki, 2011: Predictability of an atmospheric blocking event that occurred on 15 December 2005. *Mon. Wea. Rev.*, **139**, 2455–2470.
- McMurdie, L., and C. F. Mass, 2004: Major numerical forecast failures over the northeast Pacific. *Wea. Forecasting*, **19**, 338–356.
- , and J. H. Casola, 2009: Weather regimes and forecast errors in the Pacific Northwest. *Wea. Forecasting*, **24**, 829–842.
- Mlawer, E. J., S. J. Taubman, P. D. Brown, M. J. Iacono, and S. A. Clough, 1997: Radiative transfer for inhomogeneous atmosphere: RRTM, a validated correlated-k model for the longwave. *J. Geophys. Res.*, **102** (D14), 16663–16682.
- Murphy, J. M., 1988: The impact of ensemble forecasts on predictability. *Quart. J. Roy. Meteor. Soc.*, **114**, 463–493.
- Piccolo, C., 2011: Growth of forecast errors from covariances modeled by 4DVAR and ETKF methods. *Mon. Wea. Rev.*, **139**, 1505–1518.
- Reynolds, C. A., and R. Gelaro, 2001: Remarks on Northern Hemisphere forecast error sensitivity from 1996 to 2000. *Mon. Wea. Rev.*, **129**, 2145–2153.
- Shapiro, M. A., H. Wernli, N. A. Bond, and R. Langland, 2001: The influence of the 1997–99 El Niño–Southern Oscillation on extratropical baroclinic life cycles over the eastern North Pacific. *Quart. J. Roy. Meteor. Soc.*, **127**, 331–342.
- Skamarock, W. C., and Coauthors, 2008: A description of the Advanced Research WRF version 3. NCAR Tech. Note TN-475, 113 pp.
- Torn, R. D., 2010: Ensemble-based sensitivity analysis applied to African easterly waves. *Wea. Forecasting*, **25**, 61–78.
- , and G. J. Hakim, 2008a: Performance characteristics of a pseudo-operational ensemble Kalman filter. *Mon. Wea. Rev.*, **136**, 3947–3963.
- , and —, 2008b: Ensemble-based sensitivity analysis. *Mon. Wea. Rev.*, **136**, 663–677.
- , —, and C. Snyder, 2006: Boundary conditions for limited-area ensemble Kalman filters. *Mon. Wea. Rev.*, **134**, 2490–2502.
- Wedam, G. B., L. A. McMurdie, and C. F. Mass, 2009: Comparison of model forecast skill of sea level pressure along the East and West Coasts of the United States. *Wea. Forecasting*, **24**, 843–854.
- Whitaker, J. S., and T. M. Hamill, 2002: Ensemble data assimilation without perturbed observations. *Mon. Wea. Rev.*, **130**, 1913–1924.
- Zheng, M., E. K. M. Chang, and B. Colle, 2013: Ensemble sensitivity tools for assessing extratropical cyclone intensity and track predictability. *Wea. Forecasting*, **28**, 1133–1156.